Supporting Information

Exploring high-performance integration in plastic crystal/film with switching and semiconducting behavior

Zhi-Xu Zhang,[a] Tie Zhang,[a] Ping-Ping Shi,[a] Wan-Ying Zhang,[b] Qiong Ye*[a] and Da-Wei Fu*[ab]

([a] Ordered Matter Science Research Center, Jiangsu Key Laboratory for Science and Applications of Molecular Ferroelectrics, Southeast University, Nanjing 211189, P.R. China

[b] Institute for Science and Applications of Molecular Ferroelectrics, Department of Chemistry, Zhejiang Normal University, 688 Yingbin Road, Jinhua 321004, P.R. China)

Table of Content

Experimental Measurement Methods

Infrared spectra and Powder X-ray diffraction. Infrared (IR) spectra were measured on a Shimadzu IR Prestige-21 in the 4000-500 cm^{-1} regions with KBr pellets as background. Powder X-ray diffraction (PXRD) measurements were performed on a Rigaku D/MAX 2000 PC X-ray diffraction system in the 2θ range of 5°–50° with a step size of 0.02°.

Thermal analysis measurements. Differential scanning calorimetry (DSC) measurements were recorded on a NETZSCH DSC 200F3 instrument by heating and cooling crystalline samples (16.3 mg) with a rate of 10 K min^{-1} from 170 K to 310 K under in aluminum crucibles at nitrogen atmosphere.

Dielectric properties measurements. The complex dielectric permittivity curves were measured on an automatic impedance Tonghui 2828 analyzer from 173 K to 310 K in the frequency range from 10 kHz to 1 MHz with an applied voltage of 1.0 V. Dielectric studies were performed on pressed-powder pellets and single crystal samples, and conductive carbon/silver glue was deposited on the surface of electrode to simulate parallel plate capacitors.

Hirshfeld surfaces analysis. Molecular Hirshfeld surface calculations were performed by using the CrystalExplorer17.5 program. When the inputting structure file in CIF format were read into the CrystalExplorer program for analysis, all bond lengths to hydrogen were automatically modified to typical standard neutron values. In this study, all the Hirshfeld surfaces were generated using a standard (high) surface resolution. The 3D d_{norm} surfaces mapped by using a fixed color scale of -0.1153 to 2.2943 Å. The 2D fingerprint plots displayed by using the 1.0-2.8 Å view with the d_e and d_i distance scales displayed on the graph axes.

Ultraviolet−Visible (UV−Vis) absorption Spectrum. Ultraviolet–visible (UV–vis) diffuse reflectance spectroscopy of $(NNDP)_3Bi_2Cl_9$ was measured on polycrystalline samples by using Shimadzu (Tokyo, Japan) UV-2600 spectrophotometer in the range of 200–900 nm at room temperature (Figure S8). $BaSO_4$ was used as the 100% reflectance reference. Powdered crystals of $(NNDP)_3Bi_2Cl_9$ were used for the measurements. The optical band gap (*E*g) of the compound was estimated by converting reflectance data to absorbance by the Kubelka–Munk equation:

$$F(R_\infty) = (1 - R_\infty)^2/2R_\infty$$

The *E*g can be obtained from Tauc equation:

$$[hv \cdot F(R_\infty)]^{1/n} = A(hv - Eg)$$

where *h* is Planck constant, *v* is the frequency of vibration, A is the proportional constant, $F(R_\infty)$ is the Kubelka−Munk function, and n represents the nature of the sample's transition, n = 1/2 for direct and n = 2 for indirect transition. The *E*g can be obtained from a Tauc plot by plotting $[hv \cdot F(R_\infty)]^{1/n}$ against the energy in electron volt.

Theoretical Calculation. The electronic band structures and the density of states of $(NNDP)_3Bi_2Cl_9$ were performed based on density functional theory (DFT) by using the CASTEP module in the Materials Studio software (Accelrys, San Diego, CA, USA). The theoretical mode was constructed by using the crystal structure data at 188 K. Perdew-Burke-Ernzerhof was used to deal with the exchange and correlation effects in the generalized gradient approximation. The core–electron interactions were described by the norm-conserving pseudo-potential. The energy cutoff and the convergence threshold were set to 800 eV and 10^{-6} eV per atom, respectively. In addition, the other parameters and convergent criteria were the default values of CASTP module code.

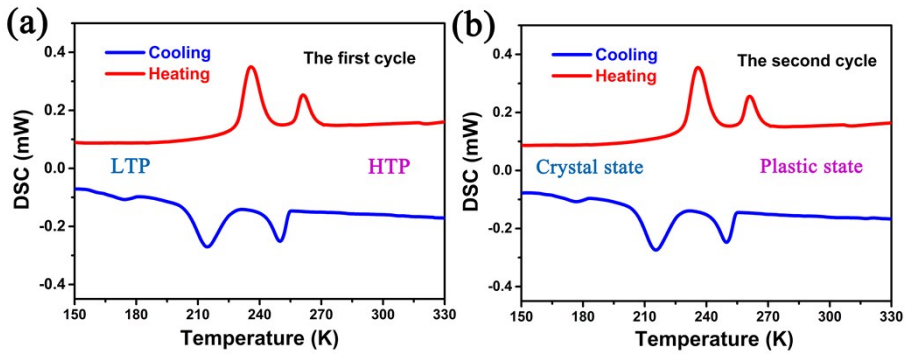

Fig. S1 DSC curves of $(NNDP)_3Bi_2Cl_9$ in cooling/heating runs at two consecutive cycles. The crystal state is the LTP mentioned in the manuscript, and the ITP and HTP corresponds to plastic state.

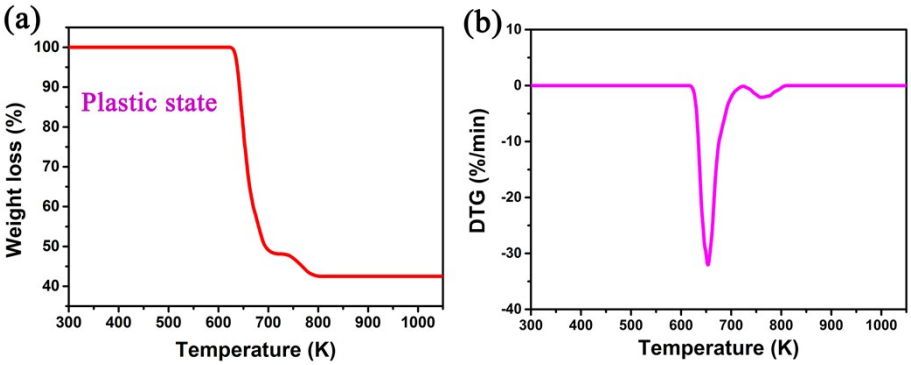

Fig. S2 (a) TG curve and (b) DTG curve of $(NNDP)_3Bi_2Cl_9$.

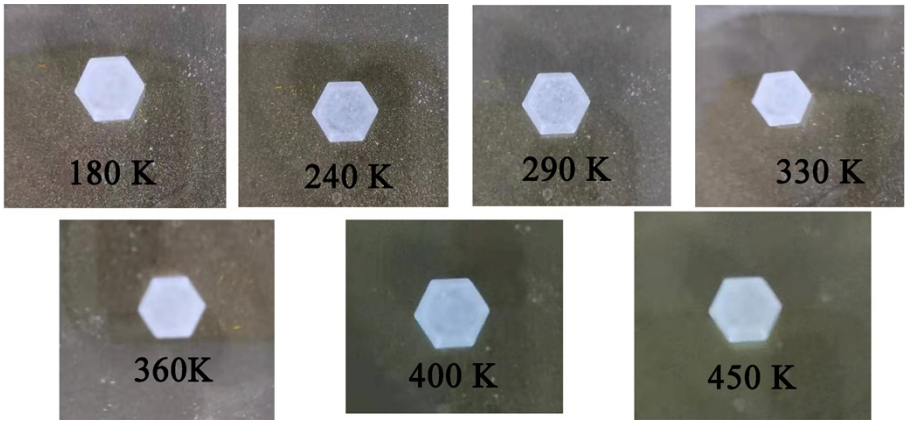

Fig. S3 The photos of the crystal in different temperature.

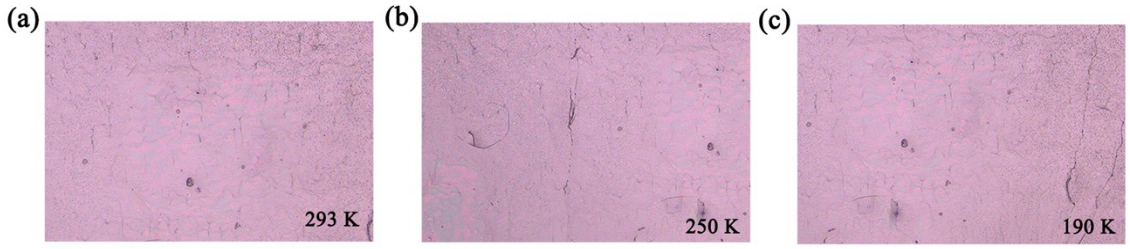

Fig. S4 The micron-sized crystal morphology of the as-prepared thin film shown by an inverted polarizing microscope.

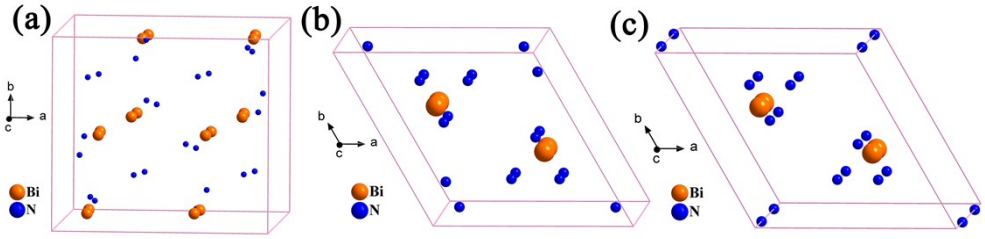

Fig. S5 Schematic representation of the positions of the N and Bi atoms at (a) LTP, (b) ITP, and (c) HTP, with other atoms omitted for clarity. Pink lines represent cell edges.

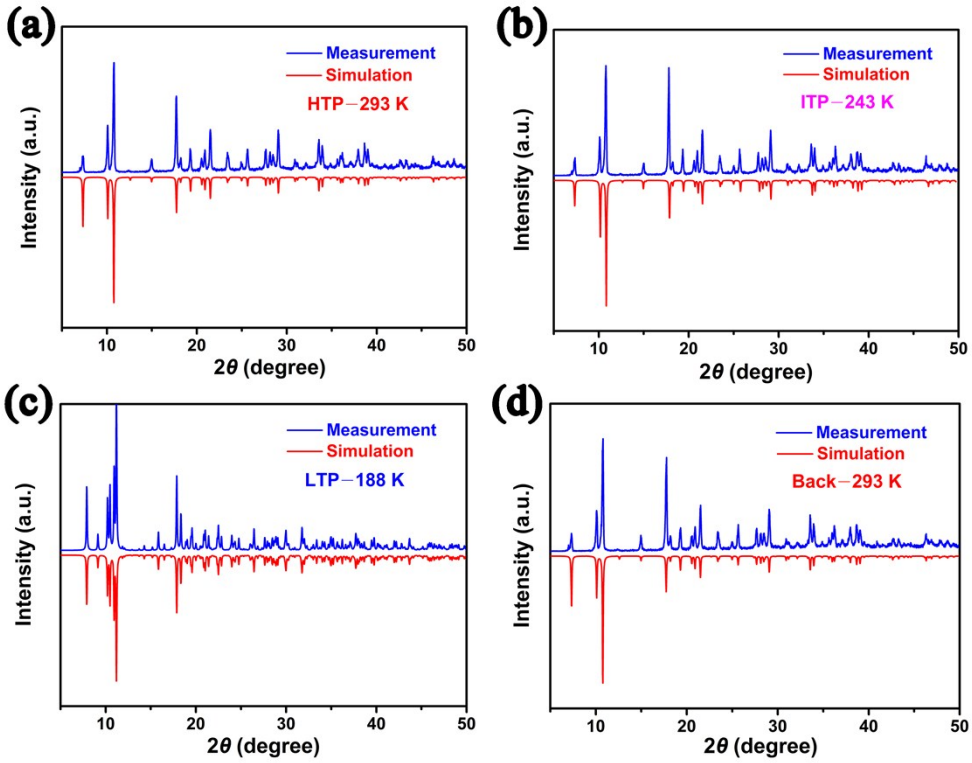

Fig. S6 Patterns of the powder X-rays diffraction (PXRD) of $(NNDP)_3Bi_2Cl_9$ at (a) 298 K, (b) 243 K, (c) 188 K and (d) back to 293 K. The measured PXRD patterns match well

with the simulated ones, verifying the purity of the bulk phase and the reversibility of structural phase transition.

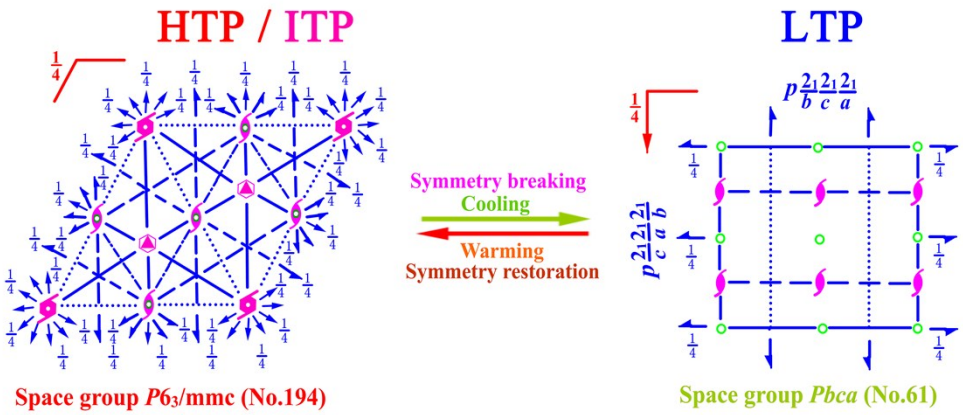

Fig. S7 Spatial symmetry operation changes of $(NNDP)_3Bi_2Cl_9$ from the HTP ($P6_3/mmc$) to LTP ($Pbca$).

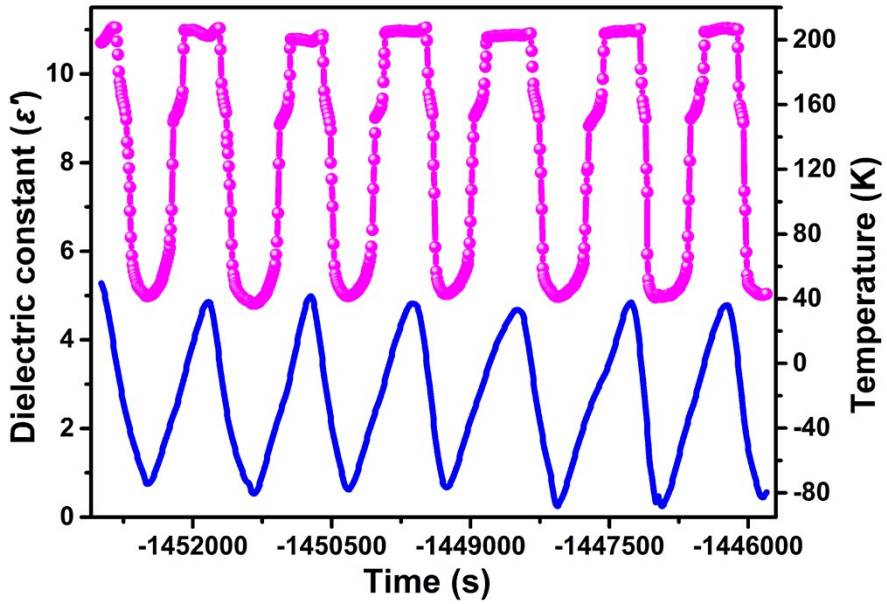

Fig. S8 Reversible switching effect of dielectric constant on polycrystalline of $(NNDP)_3Bi_2Cl_9$ (pink line). And the corresponding temperature curve is blue line, indicating the relationship of dielectric switching curves and temperature profiles over time is matched the switches.

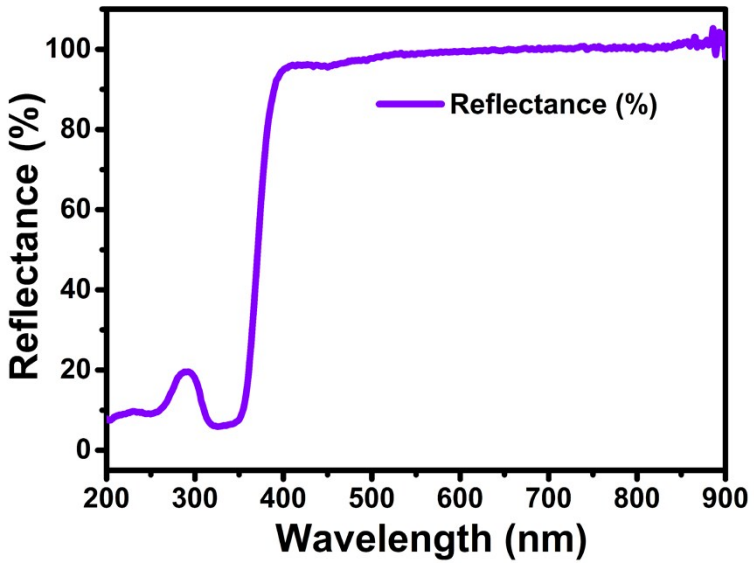

Fig. S9 UV-vis reflectance spectra of $(NNDP)_3Bi_2Cl_9$.

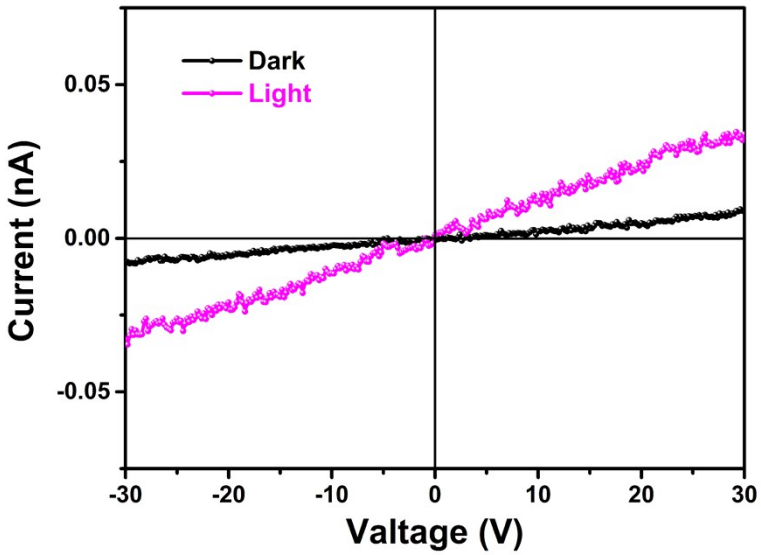

Fig. S10 The *I-V* curves performed on a single crystal of $(NNDP)_3Bi_2Cl_9$ under dark and simulated sunlight.

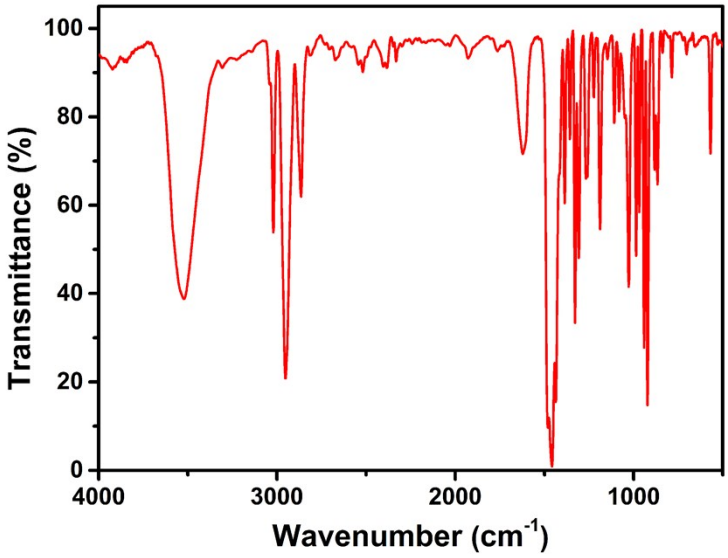

Fig. S11 IR spectra of $(NNDP)_3Bi_2Cl_9$ recorded at the spectral range 4000-500 cm^{-1}.

Dielectric permittivity matrix

Considering the point group *mmm* of $(NNDP)_3Bi_2Cl_9$ in its LTP, the dielectric constant matrix [ε] can be written as:

$$\begin{bmatrix} \varepsilon_{11} & 0 & 0 \\ 0 & \varepsilon_{22} & 0 \\ 0 & 0 & \varepsilon_{33} \end{bmatrix}_3$$

In ITP and HTP, $(NNDP)_3Bi_2Cl_9$ located in the point group $P6_3/mmc$, the dielectric constant matrix [ε] can be written as:

$$\begin{bmatrix} \varepsilon_{11} & 0 & 0 \\ 0 & \varepsilon_{11} & 0 \\ 0 & 0 & \varepsilon_{33} \end{bmatrix}_2$$

The element ε_{11}, ε_{22} and ε_{33} are the longitudinal dielectric coefficient, which characterizes the dielectricity as response to an applied electric field in the same direction.

Table S1. Crystal data and structure refinements for $(NNDP)_3Bi_2Cl_9$ at 188 K, 243 K and 293 K.

	LTP (188K)	ITP (243K)	HTP (293K)
Empirical formula	$C_{21}H_{48}N_3Bi_2Cl_9$	$C_{21}H_{48}N_3Bi_2Cl_9$	$C_{21}H_{48}N_3Bi_2Cl_9$
Formula weight	1079.63	1079.63	1079.63
Crystal system	Orthorhombic	Hexagonal	Hexagonal
Space group	*Pbca*	*P*6(3)/*mmc*	*P*6(3)/*mmc*
a (Å)	19.3244(4)	9.7668(3)	9.8365(4)
b (Å)	17.3194(4)	9.7668(3)	9.8365(4)
c (Å)	22.3457(5)	23.2252(10)	23.2129(11)
α (°)	90.00	90.00	90.00
β (°)	90.00	90.00	90.00
γ (°)	90.00	120.00	120.00
Volume($Å^3$)	7478.8(3)	1918.64(14)	1945.10(14)
Z	8	2	2
Radiation type	Mo-Kα	Mo-Kα	Mo-Kα
Absorption correction	Multi-scan	Multi-scan	Multi-scan
Calculated density	1.918	1.785	1.761
F (000)	4112	932	932
θ range for data collection	2.41–26.0°	2.41–27.48°	2.55–27.48°
Reflections collected/unique	43267 / 7339	10201 / 887	9766 / 900
R (int)	0.047	0.040	0.038
Goodness-of-fit on F^2	1.023	1.178	1.025
$R_1[I > 2\sigma(I)]$	0.0263	0.1701	0.0499
w$R_2[I > 2\sigma(I)]$	0.0620	0.3321	0.1881

Table S2. Selected lengths [Å] for $(NNDP)_3Bi_2Cl_9$ at 188 K, 243 K and 293 K.

Temperature	bond lengths [Å]			
188 K	Bi1–Cl1	2.5917 (10)	Bi2–Cl4	2.9736 (10)
	Bi1–Cl2	2.5746 (10)	Bi2–Cl5	2.8907 (10)
	Bi1–Cl3	2.6110 (11)	Bi2–Cl6	2.9145 (11)
	Bi1–Cl4	2.8720 (10)	Bi2–Cl7	2.5741 (10)
	Bi1–Cl5	2.8958 (10)	Bi2–Cl8	2.5909 (10)
	Bi1–Cl6	2.8246 (10)	Bi2–Cl9	2.5458 (10)
243 K	Bi2–Cl1	2.566 (10)	Bi2–Cl2^{vii}	2.871 (6)
	Bi2–Cl1^{v}	2.566 (10)	Bi2–Cl2	2.871 (6)
	Bi2–Cl1^{vi}	2.566 (10)	Cl2–Bi2^{vii}	2.871 (6)

293 K	Bi1–Cl1	2.564 (4)	Bi1–Cl2	2.887 (3)
	Bi1–Cl1^{viii}	2.564 (4)	Bi1–Cl2^{viii}	2.887 (3)
	Bi1–Cl1^{ix}	2.564 (4)	Bi1–Cl2^{ix}	2.887 (3)

Table S3. Selected angles [°] for $(NNDP)_3Bi_2Cl_9$ at 188 K, 243 K and 293 K.

Temperature	bond angles [°]			
188 K	Cl2–Bi1–Cl1	90.40 (3)	Cl9–Bi2–Cl7	93.48 (4)
	Cl2–Bi1–Cl3	93.28 (3)	Cl9–Bi2–Cl8	89.84 (3)
	Cl1–Bi1–Cl3	92.72 (4)	Cl7–Bi2–Cl8	93.32 (3)
	Cl2–Bi1–Cl6	91.93 (3)	Cl9–Bi2–Cl5	87.54 (3)
	Cl1–Bi1–Cl6	93.30 (3)	Cl7–Bi2–Cl5	98.43 (3)
	Cl3–Bi1–Cl6	172.01 (3)	Cl8–Bi2–Cl5	168.09 (3)
	Cl2–Bi1–Cl4	93.43 (3)	Cl9–Bi2–Cl6	98.11 (3)
	Cl1–Bi1–Cl4	172.42 (3)	Cl7–Bi2–Cl6	168.26 (3)
	Cl3–Bi1–Cl4	93.59 (3)	Cl8–Bi2–Cl6	88.60 (3)
	Cl6–Bi1–Cl4	80.05 (3)	Cl5–Bi2–Cl6	80.27 (3)
	Cl2–Bi1–Cl5	172.09 (3)	Cl9–Bi2–Cl4	166.52 (3)
	Cl1–Bi1–Cl5	94.62 (3)	Cl7–Bi2–Cl4	91.33 (3)
	Cl3–Bi1–Cl5	92.58 (3)	Cl8–Bi2–Cl4	102.45 (3)
	Cl6–Bi1–Cl5	81.70 (3)	Cl5–Bi2–Cl4	79.30 (3)
	Cl4–Bi1–Cl5	80.91 (3)	Cl6–Bi2–Cl4	76.95 (3)
	Bi1–Cl4–Bi2	83.31 (2)	Bi1–Cl6–Bi2	85.23 (3)
	Bi2–Cl5–Bi1	84.38 (2)		
243 K	Cl1–Bi2–Cl1^{v}	92.1 (3)	Cl1^{vi}–Bi2–Cl2^{vii}	171.8 (2)
	Cl1–Bi2–Cl1^{vi}	92.1 (3)	Cl2^{v}–Bi2–Cl2^{vii}	80.06 (17)
	Cl1^{v}–Bi2–Cl1^{vi}	92.1 (3)	Cl1–Bi2–Cl2	171.8 (2)
	Cl1–Bi2–Cl2^{v}	93.66 (18)	Cl1^{v}–Bi2–Cl2	93.66 (18)
	Cl1^{v}–Bi2–Cl2^{v}	171.8 (2)	Cl1^{vi}–Bi2–Cl2	93.66 (18)
	Cl1^{vi}–Bi2–Cl2^{v}	93.66 (18)	Cl2^{v}–Bi2–Cl2	80.06 (17)
	Cl1–Bi2–Cl2^{vii}	93.66 (18)	Cl2^{vii}–Bi2–Cl2	80.06 (17)
	Cl1^{v}–Bi2–Cl2^{vii}	93.66 (18)	Bi2^{vii}–Cl2–Bi2	84.1 (2)

293 K	$Cl1^{viii}$–Bi1–$Cl1^{ix}$	91.70 (15)	Cl1–Bi1–$Cl2^{ix}$	93.78 (10)
	$Cl1^{viii}$–Bi1–Cl1	91.70 (15)	$Cl1^{ix}$–Bi1–Cl2	172.14 (12)
	$Cl1^{ix}$–Bi1–Cl1	91.70 (15)	Cl1–Bi1–$Cl2^{viii}$	172.14 (12)
	$Cl1^{viii}$–Bi1–Cl2	93.78 (10)	$Cl1^{viii}$–Bi1–$Cl2^{ix}$	172.14 (12)
	Cl1–Bi1–Cl2	93.78 (10)	Cl2–Bi1–$Cl2^{viii}$	80.24 (9)
	$Cl1^{viii}$–Bi1–$Cl2^{viii}$	93.78 (10)	Cl2–Bi1–$Cl2^{ix}$	80.24 (9)
	$Cl1^{ix}$–Bi1–$Cl2^{viii}$	93.78 (10)	$Cl2^{viii}$–Bi1–$Cl2^{ix}$	80.24 (9)
	$Cl1^{ix}$–Bi1–$Cl2^{ix}$	93.78 (10)	Bi1–Cl2–$Bi1^{vii}$	83.84 (12)

Symmetry codes:

188 K (i) *x*, −*y*+1/2, *z*+1/2; (ii) −*x*+1/2, *y*−1/2, *z*; (iii) −*x*, *y*−1/2, −*z*+1/2; (iv) *x*, −*y*+1/2, *z*−1/2; (v) *x*+1/2, *y*, −*z*+1/2.

243 K (i) −y+1, x−y−1, z; (ii) −x+y+2, −x+1, z; (iii) −x+y+2, −x+1, −z+3/2; (iv) x, y, −z+3/2; (v) −y+1, x−y+1, z; (vi) −x+y, −x+1, z; (vii) −x+y, −x+1, −z+3/2; (viii) −x+y+1, −x+1, z; (ix) −y+1, x−y, z; (x) −y+1, x−y−1, −z+3/2.

293 K (i) −*x*+*y*+1, −*x*+1, *z*; (ii) −*y*+1, *x*−*y*, *z*; (iii) −*x*+*y*, −*x*, *z*; (iv) −*y*, *x*−*y*, *z*; (v) −*x*+*y*, −*x*, −*z*+3/2; (vi) −*y*, *x*−*y*, −*z*+3/2; (vii) *x*, *y*, −*z*+3/2; (viii) −*x*+*y*, −*x*+1, *z*; (ix) −*y*+1, *x*−*y*+1, *z*.

Table S4 Equivalent isotropic displacement parameters for $(NNDP)_3Bi_2Cl_9$ at 188 K, 243 K and 293 K.

Temperature		Uiso (Å^2)		
188 K	Bi1	0.024(5)	C6	0.044(12)
	Bi2	0.023(5)	C7	0.044(11)
	Cl1	0.037(2)	C8	0.043(11)
	Cl2	0.033(2)	C9	0.061(15)
	Cl3	0.041(3)	C10	0.090(2)
	Cl4	0.034(2)	C11	0.102(3)
	Cl5	0.032(2)	C12	0.072(18)
	Cl6	0.034(2)	C13	0.061(15)
	N1	0.027(7)	C14	0.045(12)
	N2	0.033(8)	C15	0.038(10)
	N3	0.031(8)	C16	0.043(11)
	C1	0.036(10)	C17	0.045(12)
	C2	0.041(11)	C18	0.046(12)

	C3	0.037(10)	C19	0.041(11)
	C4	0.035(10)	C20	0.053(13)
	C5	0.028(9)	C21	0.050(12)
243 K	Bi2	0.077(5)	C2	0.276(4)
	Cl1	0.158(3)	C3	0.263(4)
	Cl2	0.092(2)	C4	0.283(19)
	N1	0.273(6)	C8	0.310(4)
	N2	0.310(3)	C9	0.311(3)
	C1	0.282(6)	C10	0.313(8)
293 K	Bi1	0.101(5)	C3	0.259(17)
	Cl1	0.187(18)	C4	0.258(19)
	Cl2	0.128(13)	C5	0.239(13)
	N1	0.253(14)	C6	0.600(3)
	N2	0.630(4)	C7	0.600(3)
	C1	0.310(2)	C8	0.590(3)
	C2	0.300(19)		